Identifying the cellular interactome of Epstein-Barr virus lytic regulator Zta reveals cellular targets contributing to viral replication

Article (Accepted Version)

Identifying the cellular interactome of Epstein-Barr virus lytic regulator Zta reveals cellular targets contributing to viral replication.

Yaqi Zhou[1,3], Kate Heesom[2], Kay Osborn[1], Rajaei AlMohammed[1,4], Steve M. Sweet[1,5], and Alison J. Sinclair[1*]

[1]School of Life Sciences, University of Sussex, Brighton BN1 9QG, UK.

[2]University of Bristol Proteomics Facility, University of Bristol, BS8 1QU, UK.

[3]Current address: Department of Otorhinolaryngology Head and Neck Surgery, Peking University Shenzhen Hospital, Shenzhen, China.

[4]Current address: Centre for Gene Regulation and Expression, School of Life Sciences, University of Dundee, DD1 5EH, UK.

[5]Current address: AstraZeneca, Clinical Proteomics, Translational Oncology, Gaithersburg, MD, USA.

*corresponding author: Prof A. J. Sinclair, School of Life Sciences, University of Sussex, Brighton BN1 9QG, UK; a.j.sinclair@sussex.ac.uk; (+44) 01273 678 194.

Abstract: 211/250

The human gamma herpesvirus Epstein-Barr virus (EBV; HHV4), infects most adults and is an important contributor to the development of many types of lymphoid and epithelial cancers. Essential contributions of viral genes to viral replication are known, but the potential contributions of cell genes are less well delineated. A key player is the viral protein Zta (BZLF1, ZEBRA, Z). This sequence-specific DNA-binding protein can disrupt EBV latency by driving the transcription of target genes and by interacting with the EBV lytic origin of

replication. Here we used an unbiased proteomics approach to identify the Zta-interactome in cells derived from a Burkitt's lymphoma. Isolating Zta and associated proteins from Burkitt's lymphoma cells undergoing EBV replication, followed by Tandem Mass Tag (TMT) mass spectrometry resulted in the identification of thirty-nine viral and cellular proteins within the Zta interactome. An association of Zta with the cellular protein NFATc2 was validated in independent experiments. Furthermore, the ability of Zta to attenuate the activity of an NFAT-dependent promoter was shown which suggests a functional consequence for the association. The expression of Zta is itself regulated through NFAT activity, suggesting that Zta may contribute to a feed-back loop that would limit its own expression, thus aiding viral replication by preventing the known toxic effects of Zta overexpression.

Data are available: ProteomeXchange PXD013727.

Importance: 124/150

Epstein-Barr virus, infects most people across the world and causes several kinds of cancer. Zta is an important viral protein that makes the virus replicate by binding to its DNA and turning on the expression of some genes. We used a sensitive, unbiased approach to isolate and identify viral and cellular proteins that physically interact with Zta. This revealed thirty-nine viral and cellular proteins. We found that one protein termed NFATc2, was already known to be important for a very early step in viral replication. We identify that once this step has occurred, Zta reduces the effectiveness of NFATc2 and suggest that this is

important to prevent cells from dying before viral replication is complete and the mature virus is released from the cells.

Introduction

Epstein-Barr virus (EBV) establishes life-long latency in memory B-cells following primary infection (1, 2). The virus is reactivated from latency to undergo lytic replication when the infected B-cell is activated following the presentation of its cognate antigen (3-5). A cascade of viral gene expression ensues resulting in viral genome replication, packaging and egress from cells. Zta (BZLF1, EB1, ZEBRA, Z), a viral transcription factor that often works in consort with a second viral transcription factor Rta (BRLF1), activates the expression of many of these lytic cycle genes (6). Genome-wide analyses of Zta and Rta binding sites reveal many viral genes that are direct targets for transactivation (7-9). In addition to this important role, Zta binds to the lytic origin of viral genome replication (OriLyt) (7, 8, 10-12). Lytic genome replication is achieved by the action of additional six viral genes (13), with potential additional contributions from cellular proteins. In addition to binding to the viral genome at OriLyt, Zta interacts with some viral protein components of the EBV replisome (13), potentially facilitating the formation of the functional replisome at OriLyt.

Viral replication is inextricably linked to the cellular environment, but the precise contributions of cellular proteins to EBV replication are unclear. Unbiased proteomics screens have identified many cellular proteins that interact with Zta. For mtSSB (14), 53BP1 (15), TORC2 (16) and INO80 (17), evidence from gene knock-down approaches shows that each gene contributes to the ability of EBV to replicate within a cell.

Here we sought to identify cellular proteins that interact with full-length Zta protein during authentic viral lytic replication, following the application of a physiologically relevant stimulus to latently infected B-cells. We anticipated that this may identify cellular proteins that contribute to any stage of EBV lytic replication, including but not exclusive to known transcription and DNA replication functions of Zta. This unbiased screen identified thirty-nine candidate proteins: seven viral and thirty-two cellular. The validity of the data set is shown by the inclusion of previously identified targets of Zta and our demonstration of the relevance of a novel component (NFATc2) for efficient EBV lytic replication.

Results

Isolation of the Zta interactome in Akata BL cells

An EBV positive Burkitt's lymphoma cell line (Akata), that harbours a latent EBV genome, was stimulated to enter lytic replication by cross-linking the surface B cell receptor (BCR) using anti-human immunoglobulin IgG, to mimic the physiologically relevant event of antigen recognition (3). Entry into lytic cycle was demonstrated by evaluating the expression of Zta protein (**Fig. 1A**) and changes in the abundance of the EBV genome (**Fig. 1B**). Analysis of the total population of cells entering early and late lytic cycle was also monitored by fluorescent activated cell sorting for Zta and gp110 (BALF4; VCA) respectively (data not shown).

The major challenge to isolating the Zta interactome lie with its strong DNA-association. Native cell lysis results in low yields of Zta, yet harsh conditions are likely to dissociate the sought-for interactions. Zta-bound DNA has been previously extracted from cells combining

the use of an in-cell cross-linking agent, formaldehyde, followed by a harsh ionic detergent (8, 18, 19). Here we sought a compromise approach. We used dithiobis-succinimidyl propionate) (DSP), a bi-functional amine-reactive cross-linker with a spacer arm of (12Å) to undertake in-cell cross-linking of proteins. This promoted the formation of high molecular weight Zta-complexes, which can be released by subsequent reduction (data not shown). Following cross-linking, proteins were extracted into a non-denaturing buffer from the insoluble chromatin by digesting the chromatin with DNase.

This approach was used to isolate the Zta-interactome from Akata cells undergoing lytic replication. Two controls were designed to enable reliable identification of the Zta interactome: extracts from latent Akata cells, precipitated with Zta antibody; and extracts from Akata cells induced to enter lytic replication, precipitated with a control antibody. Repeat experiments were undertaken in triplicate (**Fig. 1C**). Each of the nine samples were labelled with a different tandem mass tag (TMT) -reagent and processed for mass spectrometry. Proteins that were enriched >2 fold compared to each control ($p \leq 0.05$) were classified as specifically interacting with Zta in the lytic cycle (**Fig. 1D**).

Analysis of the proteins in the Zta-interactome

As anticipated, Zta was the highest scoring protein identified during the proteomic analysis (**Fig. 1D**). In addition, seven viral proteins displayed reproducibly ($p \leq 0.05$) high ratios in the Zta immunoprecipitation compared to either control (**Table 1**). Of these, both BGLF4 and BALF5 have been shown to interact with Zta previously (10, 20, 21). The identification of these proteins provides a validation of the experimental approach.

Thirty-two cellular proteins were also reproducibly ($p \leq 0.05$) enriched more than two-fold in the Zta precipitation when compared to both controls (**Table 2**). Analysis of common Gene Ontology (Biological Processes) revealed an enrichment for proteins involved in transcription, the nucleus and nucleoplasm (**Fig. 2 and Table S1**). Of these functionally related proteins, one was chosen for further analysis NFATc2.

Contribution of NFATc2 to EBV replication

NFATc2 encodes a transcription co-factor that is activated through calcium mediated signal transduction following dephosphorylation by calcineurin. It acts together with the AP1 transcription factor to activate gene expression via a composite DNA element ARRE2 (22-24). Using immunoprecipitation with non-cross-linked protein extracts from Akata cells induced to initiate EBV lytic cycle, we demonstrate the co-precipitation of NFATc2 with Zta antibodies (**Fig. 3A**). To probe the specificity of the interaction further, we undertook additional immune precipitation experiments with two other nuclear DNA binding proteins expressed in B-cells, EBF1 and LEF1. Neither of these co-precipitated NFATc2 protein (**Fig. 3B-C**).

To explore the contribution of NFATc2 to his-Zta mediated transcriptional regulation, we used a Zta-responsive viral reporter, BHFL1p luciferase (**Fig. 4**). This promoter is transactivated by over 200-fold when introduced into cells with a hisZta expression vector. When PMA and ionomycin are added to stimulate the activation of NFATc2/AP1, there is little impact on either basal transcription or Zta-mediated activation (**Fig. 4 A-C**). This suggests that the NFATc2 interaction with Zta does not result in an alteration of the

transactivation potential of Zta. To explore this further, the endogenous abundance of NFATc2 was decreased using a smart Si RNA pool against NFAT genes and the impact on Zta-mediated activation of BHLF1p determined. Although the smart pool reduced NFATc2 protein abundance by 66%, there was no consequent decrease in the ability of Zta to activate gene expression (**Fig. 4 D-F**).

An NFAT reporter assay was used to ask the reciprocal question, whether an NFAT-dependent promoter was impacted by the expression of hisZta (**Fig. 5A**). The NFAT reporter pGL3 NFAT-luciferase was introduced into DG75 B-cells with control SiRNA or the smart Si RNA pool against NFAT genes. As anticipated, the combination of both Ionomycin and PMA lead to a substantial increase in transcriptional activation of the NFAT reporter. The inclusion of the NFAT Si RNA smart pool resulted in a ~50% reduction in the expression of both NFATc1 and NFATc2. A similar decrease in Ionomycin and PMA driven promoter activity was observed when the NFAT smart Si RNA pool was co-expressed (**Fig. 5 B-C**). This confirms that the Ionomycin and PMA stimulation of the pGL3 NFAT-luciferase promoter is regulated by NFAT in these cells.

The inhibitor FK506 blocks the activation of calcineurin and JNK (25), thereby inhibiting activation of NFATc2/AP1; this was used here to identify calcineurin- and JNK-dependent regulatory events. The increased NFAT reporter promoter activity stimulated by Ionomycin and PMA was negated by the addition of FK506 as expected (**Fig. 5D**). Co-transfection of hisZta with the NFAT reporter resulted in a rise in basal promoter activity. As AP1 sites have some similarity of sequence with ZREs, we questioned whether Zta may act directly through ARRE2. We analysed the composite NFAT/AP1 site in this reporter for known Zta binding

sites (26) and we evaluated the potential for Zta to bind to the element using *in vitro* DNA binding assays (**Fig. 6**). Neither line of investigation provided support for a direct Zta DNA-interaction with this promoter. Zta also interacts with components of the basal transcriptional machinery including the TATA-binding protein TFIID (27), and we suggest that the increase in basal expression may result from this. When the impact of hisZta expression on promoter activation observed following ionomycin and PMA was assessed, hisZta was shown to significantly and substantially reduce this activation by 25 fold (**Fig. 5C-D**). The impact of hisZta expression is also reflected when considering the ionomycin and PMA stimulated cells and comparing the difference of NFAT-dependent promoter activity in the presence and absence of hisZta expression where a significant reduction in activity is also observed.

Discussion

The identification of the Zta interactome opens a new avenue of understanding of Zta function during the EBV lytic replication cycle. The identification of two previously known targets of Zta (BGLF4 and BALF5) provides robust confirmation of the relevance of these targets and the additional proteins.

Of the five novel viral proteins, three are found in the viral capsid. The portal protein, BBRF1, is a homologue of HSV-1 UL6, which is required for the encapsulation and cleavage of the viral genome. Specifically, the deletion of BBRF1 from the EBV genome has been shown to result in 'empty' capsids containing no viral genome (28) and transmission electron microscopy of BBRF1 revealed the formation of a self-assembling structure consistent with other herpesvirus portals (29). Two further capsid proteins BVRF2, a

protease, and BcLF1, the major capsid protein, are both required for the EBV capsid assembly (30). Interaction of Zta with these three capsid proteins suggested that, in addition to its well-characterized role in events leading to EBV genome replication, Zta might have additional roles downstream of genome replication, relating to the assembly or function of the capsid.

The importance of calcium signalling to the disruption of latency by reactivation of the EBV lytic cycle following immunoglobulin stimulation is well established; inhibitors of critical aspects of Ca^{2+}-mediated signal transduction pathways, cyclosporin A (CsA) and Tarcolimus (FK506) that converge on the inhibition of the Ca^{2+}-dependent phosphatase calcineurin, both block EBV lytic reactivation (31). Calcium signalling acts on the BZLF1 promoter through many routes including the actions of TORC2 and MEF2 (32). Recently, enhanced EBV lytic cycle reactivation was identified in cancer-associated EBV strains and a sequence variation within the BZLF1 promoter that forms a functional response element for the NFAT transcription factor was found to contribute an additional route for activation through calcium signal transduction (33).

We were therefore intrigued to identify NFATc1 and NFATc2 as members of the Zta interactome. NFAT has four family members, that are activated by dephosphorylation by the Ca^{2+}-dependent phosphatase calcineurin, resulting in nuclear translocation followed by direct interaction with DNA response elements. The obvious approach to questioning the role of the Zta-NFAT interaction in EBV lytic cycle is to inhibit the expression of NFAT. The calcineurin inhibitor FK506 suggests a route to question the contribution of NFATs to Zta function. However, the first step in EBV reactivation, activation of Zta expression, is

controlled through Ca^{2+}-dependent signal transduction and so inhibiting calcineurin-dependent signal transduction with FK506 will both inhibit Zta activation and all subsequent Zta-dependent events (31); we confirmed that this was so for Akata cells (data not shown). We therefore used simple promoter-reporters to dissect the potential for cross-talk between Zta and the NFAT transcription factors. After validating that the PMA and ionomycin stimulation of the NFAT-dependent promoter is reliant on NFAT expression in these cells, we found that Zta attenuates NFAT-mediated activation. In contrast, NFAT does not impact on Zta-mediated activation through ZREs. This approach revealed that the impact of NFAT-Zta cross-talk is unidirectional. We propose a model whereby the attenuation of NFAT-mediated activation by Zta occurs through the protein-protein interaction between Zta and NFAT that we identified using TMT-mass spectrometry (**Fig. 7**).

The attenuation of NFAT-mediated gene activation by Zta poses a conundrum when considering the contribution of NFAT to EBV lytic reactivation. We know that inhibition by the calcineurin inhibitor FK506 prevents EBV lytic cycle reactivation, implying a positive role for calcineurin-dependent targets such as NFAT during EBV lytic reactivation. However, the attenuation of NFAT-mediated gene activation by Zta suggests that NFAT activity may be obstructive to EBV lytic cycle. A solution lies with careful consideration of the order of the events during EBV reactivation and lytic cycle. It is known that Zta expression can have negative impacts on cell viability and that during EBV lytic cycle the expression of Zta is coupled to an ordered co-expression of the anti-apoptotic viral protein v-BCL2 (BHRF1) (34). Indeed, there is evidence that Zta (BZLF1) mRNA expression is limited during the EBV lytic cycle; abundance of the transcript is known to first peak then fall following immunoglobulin

cross-linking (35). We propose that we have identified a negative feedback-loop that acts to fine-tune Zta expression during EBV lytic cycle and that this is mediated by the ability of Zta to attenuate the NFAT-activity. The Ca^{2+}-dependent signal transduction that initiates EBV lytic reactivation stimulates NFAT transcription factors to activate the BZLF1 promoter through the several DNA elements including the NFAT response element. This promotes the expression of Zta protein, which acting through interactions with its DNA-response elements directly re-programmes EBV and cellular gene expression. As Zta levels rise, we suggest that the interaction between Zta with NFATc2 results in attenuation of NFAT-dependent transcription leading to reduced Zta expression. Together this maintains the Zta abundance in cells within the required, yet tolerated zone. The direct interactions between Zta and NFATc2 suggest a novel molecular mechanism to fine-tune the expression of Zta.

Materials and Methods

Cells and transfections. Akata Burkitt's Lymphoma cells (4) and DG75 cells (36) were maintained in RPMI 1640 medium supplemented with 10% FBS, 100 units/ml penicillin, 100 µg/ml streptomycin and 2 mM L-glutamine (Fisher Scientific) at 37°C with 5% CO_2. To induce EBV lytic cycle in Akata cells, cells were re-suspended at 2 x 10^6 cells/ml in media and anti-human IgG (Dako) was added to 0.13 % (v/v) of the final volume, then incubated for 24 hours.

For promoter-reporter experiments, electroporation (Biorad) was used to introduce 5µg of BHLF1-luciferase, or GL3NFAT-luciferase together with 5µg of pcDNA3 or pcDNA3-hisZta plasmids into 1 x 10^7 DG75 cells. 48 hours later, 90µl of passive cell lysis buffer (Promega)

256 was added to the cell pellets and incubated 30 minutes on ice, then 30 minutes at room
257 temperature. Then cell lysates were centrifuged and the supernatant was transferred to
258 clean tubes. 10µl of triplicate samples were pipetted into a white 96-well plate. A Glomax
259 (Promega) multi-detection plate reader with an auto sampler, dispensed 50µl of luciferase
260 activation reagent (Promega) per well, and read output light for 10 seconds with a delay for
261 2 seconds after adding the reagent. The protein concentration in the lysates was
262 determined using a bicinchoninic acid (BCA) assay (Pierce). The concentration of each lysate
263 used to normalise the luciferase activity.
264
265 Either a smart pool of SiRNA directed against NFATc1 and c2 or the non-targeting siRNA
266 pool #1 (Dharmacon) was introduced into DG75 cells. No targeting smartpool #1 consists of
267 UAGCGACUAAACACAUCAA, UAAGGCUAUGAAGAGAUAC, AUGUAUUGGCCUGUAUUAG;
268 NFATc1 targeting smartpool UCAGAAACUCCGACAUUGA, GGACAGCUAUCCGGUCGUG,
269 GUUGAGAUCCCGCCAUUUC, AGGAAGAACACACGGGUAC; NFATc2 targeting smartpool
270 CCAAUAAUGUCACCUCGAA, GCAGAAUCGUCUCUUUACA, GCGGGGAUCUUGAAGCUUA,
271 UCAUGUACUGCGAGAAUUU. The concentration of Non-Targeting siRNA pool #1 was
272 200µM, Human NFATC1 siRNA 100µM and Human NFATc2 siRNA 100µM. 250ng of pcDNA3
273 or pcDNA3-hisZta expression vectors and 250ng of BHLF1-luciferase were delivered at the
274 same time. The Neon transfection system (100µl Neon kit) was used in this experiment. 5 x
275 10^6 cells were resuspended in 104µl Buffer T. 6µl DNA and RNA mix in each condition was
276 prepared before adding to the cells. Electroporation was performed at 1300V, 30 msec, and
277 1 pulse in 100µl Neon tip. Whole media without antibiotics was used for culturing the cells.
278 24 hours post-transfection, ionomycin (final concentration 1µM) and PMA (final
279 concentration 20ng/ml) were added as indicated, after another 48 hours, cells were

harvested and washed by D-PBS. Then 1/10 of the cells were used for western blotting and the rest of the cells were used for luciferase assay.

Cell viability was determined using Alamar Blue (Invitrogen). Following an overnight incubation, fluorescence was measured using a Glomax (Promega) plate reader with an excitation wavelength of 520nm and an emission at 580-640nm.

EBV viral load was determined using an established assay (38).

An inhibitor of Calcineurin FK506 (Sigma) was solubilised in water.

Proteins

Immunoprecipitations were carried out using lysates derived from 5 x 10^7 Akata cells without cross-linking of cells. Lysis in cell lytic reagent (Sigma) and DNAse digestion were undertaken, as for proteomics preparation. However, the anti-Zta goat antibody SCZ (Santa Cruz) was added overnight followed by addition of protein-G dynabeads without prior cross-linking of the antibody to the beads. For LEF1 immunoprecipitations rabbit LEF1 #2286s from CST was used and for EBF1, mouse EBF Antibody (C-8): sc-137065 (Santa Cruz) was used. Following washing precipitated proteins were analysed by western blot with monoclonal antibodies specific for NFATc2 (Santa Cruz) and the precipitated proteins.

For western blot analysis, protein samples were separated in 10% Bis-Tris NuPAGE gel in morpholinepropanesulfonic buffer (MOPS). Following blocking for non-specific binding, the membrane was incubated with primary antibodies at 4°C overnight, including BZ1 antibody

(a kind gift from Martin Rowe, mouse 1:200), Actin antibody (Sigma, Rabbit 1:1000), NFATc2 (Santa Cruz, mouse, 1:200) and GFP antibody (Invitrogen, rabbit, 1:1000). Following washing in PBS-Tween (0.1%), incubation continued with either fluorescent or enzyme-linked secondary antibodies. Donkey anti-rabbit (Licor, 800CW, 1:5000-1:10,000), goat anti-mouse (Licor, 680RD, 1:5000-1:10,000), anti-multi species conjugated HRP (VeriBlot Abcam 1:1000) were incubated for 1 hour at room temperature. The fluorescent signal was detected at either 700nm or 800nm channel by the Odyssey Fc system. The HRP-linked signal was detected with the Westernsure ECL substrate (Licor) and the Odyssey Fc imager (LI-COR).

Proteomics and immunoprecipitations

For each replicate, 1 x 10^8 Akata cells were concentrated to 1 x 10^7 cells/ml and were cross-linked following addition of 0.2mM DSP (Thermo Scientific) for 30 minutes at room temperature. The reaction was stopped by the addition of Tris solution to a final concentration of 50mM and incubated for 15 minutes, then cells were washed with D-PBS (Gibco). The cells were re-suspended in CellLytic MT cell lysis reagent (Sigma) for 10 minutes at 4°C. After centrifugation, the nuclear pellets were then re-suspended in lysis reagent (Sigma) with the addition of 250U/ml of Benzonase (Sigma). The nuclear extracts were then diluted in IP dilution buffer (0.01% SDS, 1.1% Triton X-100, 1.2 mM EDTA, 16.7 mM Tris pH 8.0, 167 mM NaCl). 10µg SCZ Zta antibody or control goat IgG were added to 25µl of protein G-dynabeads and cross-linked following the addition of bis(sulfosuccinimidyl)suberate (BS3) (Thermo Scientific). These were then incubated with the nuclear extracts and overnight at 4°C on a rotating wheel. Beads were washed by low salt, high salt, lithium buffers as described previously for Chromatin precipitation (39) and finally washed in 10 mM Tris/Cl pH 7.5; 150 mM NaCl; 0.5 mM EDTA. The final wash buffer was removed and the beads

were resuspended in 50mM triethyl ammonium bicarbonate prior to reduction (10mM TCEP, 55°C, 1h), alkylation (18.75mM iodoacetamide, ambient, 30min) and digestion with trypsin (2.5µg trypsin per sample; 37°C, overnight). Proteins were eluted in 2 X Laemmli sample buffer for 10 min at 95 °C. Samples on the beads were reduced, alkylated and digested with trypsin (2.5µg trypsin per sample; 37°C, overnight). The resulting peptides were labelled with Tandem Mass Tag (TMT) ten plex reagents according to the manufacturer's protocol (Thermo Fisher Scientific) and the labelled samples pooled. The pooled sample was evaporated to dryness and resuspended in buffer A (20mM ammonium hydroxide, pH 10) prior to fractionation by high pH reversed-phase chromatography using an Ultimate 3000 liquid chromatography system (Thermo Fisher Scientific). In brief, the sample was loaded onto an XBridge BEH C18 Column (130Å, 3.5 µm, 2.1 mm X 150 mm, Waters, UK) in buffer A and peptides eluted with an increasing gradient of buffer B (20 mM Ammonium Hydroxide in acetonitrile, pH 10) from 0-95% over 60 minutes. The resulting fractions (four in total) were evaporated to dryness and resuspended in 1% formic acid prior to analysis by nano-LC MSMS using an Orbitrap Fusion Tribrid mass spectrometer (Thermo Scientific).

High pH RP fractions were further separated using an Ultimate 3000 nanoHPLC system in line with an Orbitrap Fusion Tribrid mass spectrometer (Thermo Scientific). In brief, peptides in 1% (vol/vol) formic acid were injected onto an Acclaim PepMap C18 nano-trap column (Thermo Scientific). After washing with 0.5% (vol/vol) acetonitrile 0.1% (vol/vol) formic acid, peptides were resolved on a 250 mm × 75 µm Acclaim PepMap C18 reverse phase analytical column (Thermo Scientific) over a 150 min organic gradient, using 7 gradient segments (1-6% solvent B over 1min., 6-15% B over 58min., 15-32%B over 58min.,

352 32-40%B over 5min., 40-90%B over 1min., held at 90%B for 6min and then reduced to 1%B
353 over 1min.) with a flow rate of 300 nl min^{-1}. Solvent A was 0.1% formic acid and Solvent B
354 was aqueous 80% acetonitrile in 0.1% formic acid. Peptides were ionized by nano-
355 electrospray ionization at 2.0kV using a stainless-steel emitter with an internal diameter of
356 30 µm (Thermo Scientific) and a capillary temperature of 275°C.
357
358 All spectra were acquired using an Orbitrap Fusion Tribrid mass spectrometer (Thermo
359 Scientific), controlled by Xcalibur 2.0 software (Thermo Scientific) and operated in data-
360 dependent acquisition mode using an SPS-MS3 workflow. FTMS1 spectra were collected at
361 a resolution of 120 000, with an automatic gain control (AGC) target of 200 000 and a max
362 injection time of 50ms. Precursors were selected with an intensity threshold of 5000,
363 according to charge state (to include charge states 2-7) and with monoisotopic precursor
364 selection. Previously interrogated precursors were excluded using a dynamic window (60s
365 +/-10ppm). The MS2 precursors were isolated with a quadrupole mass filter set to a width
366 of 1.2m/z. ITMS2 spectra were collected with an AGC target of 10 000, max injection time of
367 70ms and CID collision energy of 35%. For FTMS3 analysis, the Orbitrap was operated at 50
368 000 resolution with an AGC target of 50 000 and a max injection time of 105ms. Precursors
369 were fragmented by high energy collision dissociation (HCD) at a normalised collision energy
370 of 60% to ensure maximal TMT reporter ion yield. Synchronous Precursor Selection (SPS)
371 was enabled to include up to 5 MS2 fragment ions in the FTMS3 scan.
372
373 The raw data files were processed and quantified using Proteome Discoverer software v2.1
374 (Thermo Scientific) and searched against the UniProt Human database (140000 entries) plus
375 EBV_proteome_B95_8 (UO000153037) and EBV_Proteome_GD1 (UP000103223) sequences

using the SEQUEST algorithm. Peptide precursor mass tolerance was set at 10ppm, and MS/MS tolerance was set at 0.6Da. Search criteria included oxidation of methionine (+15.9949) as a variable modification and carbamidomethylation of cysteine (+57.0214) and the addition of the TMT mass tag (+229.163) to peptide N-termini and lysine as fixed modifications. Searches were performed with full tryptic digestion and a maximum of 2 missed cleavages were allowed. The reverse database search option was enabled and all data was filtered to satisfy false discovery rate (FDR) of 5%.

The mass spectrometry proteomics data have been deposited to the ProteomeXchange Consortium via the PRIDE [1] partner repository with the dataset identifier PXD013727.

The Gene Ontology (GO) analysis were undertaken through from The Database for Annotation, Visualization and Integrated Discovery (DAVID) (https://david.ncifcrf.gov/) (40).

Acknowledgments.

This study was funded with support from the China Sussex Scholarship fund.

394 **References**

395

396 1. Epstein A. 2015. Why and How Epstein-Barr Virus Was Discovered 50 Years Ago. Curr
397 Top Microbiol Immunol 390:3-15.
398 2. Shannon-Lowe C, Rickinson AB, Bell AI. 2017. Epstein-Barr virus-associated
399 lymphomas. Philos Trans R Soc Lond B Biol Sci 372.
400 3. Takada K. 1984. Cross-linking of surface immunoglobulins induces Epstein-Barr virus
401 in Burkitt's lymphoma cell lines. Int J Cancer 33:27-32.
402 4. Takada K, Ono Y. 1989. Synchronous and sequential activation of latently infected
403 Epstein-Barr virus genomes. J Virol 63:445-9.
404 5. Takada K, Horinouchi K, Ono Y, Aya T, Osato T, Takahashi M, Hayasaka S. 1991. An
405 Epstein-Barr virus-producer line Akata: establishment of the cell line and analysis of
406 viral DNA. Virus Genes 5:147-56.
407 6. Kenney SC, Mertz JE. 2014. Regulation of the latent-lytic switch in Epstein-Barr virus.
408 Semin Cancer Biol 26:60-8.
409 7. Bergbauer M, Kalla M, Schmeinck A, Gobel C, Rothbauer U, Eck S, Benet-Pages A,
410 Strom TM, Hammerschmidt W. 2010. CpG-methylation regulates a class of Epstein-
411 Barr virus promoters. PLoS Pathog 6:e1001114.
412 8. Ramasubramanyan S, Kanhere A, Osborn K, Flower K, Jenner RG, Sinclair AJ. 2012.
413 Genome-wide analyses of Zta binding to the Epstein-Barr virus genome reveals
414 interactions in both early and late lytic cycles and an epigenetic switch leading to an
415 altered binding profile. J Virol 86:12494-502.
416 9. Heilmann AMF, Calderwood MA, Portal D, Lu Y, Johannsen E. 2012. Genome-Wide
417 Analysis of Epstein-Barr Virus Rta DNA Binding. Journal of Virology 86:5151-5164.
418 10. Baumann M, Feederle R, Kremmer E, Hammerschmidt W. 1999. Cellular
419 transcription factors recruit viral replication proteins to activate the Epstein-Barr
420 virus origin of lytic DNA replication, oriLyt. Embo Journal 18:6095-6105.
421 11. Schepers A, Pich D, Hammerschmidt W. 1993. A Transcription Factor with Homology
422 to the Ap-1 Family Links Rna-Transcription and DNA-Replication in the Lytic Cycle of
423 Epstein-Barr-Virus. Embo Journal 12:3921-3929.
424 12. Schepers A, Pich D, Hammerschmidt W. 1996. Activation of oriLyt, the lytic origin of
425 DNA replication of Epstein-Barr virus, by BZLF1. Virology 220:367-376.
426 13. Fixman ED, Hayward GS, Hayward SD. 1995. Replication of Epstein-Barr virus oriLyt:
427 lack of a dedicated virally encoded origin-binding protein and dependence on Zta in
428 cotransfection assays. J Virol 69:2998-3006.
429 14. Wiedmer A, Wang P, Zhou J, Rennekamp AJ, Tiranti V, Zeviani M, Lieberman PM.
430 2008. Epstein-Barr virus immediate-early protein Zta co-opts mitochondrial single-
431 stranded DNA binding protein to promote viral and inhibit mitochondrial DNA
432 replication. J Virol 82:4647-55.
433 15. Bailey SG, Verrall E, Schelcher C, Rhie A, Doherty AJ, Sinclair AJ. 2009. Functional
434 Interaction Between Epstein-Barr Virus Replication Protein Zta and Host DNA-
435 Damage Response Protein 53BP1. J Virol.
436 16. Murata T, Sato Y, Nakayama S, Kudoh A, Iwahori S, Isomura H, Tajima M, Hishiki T,
437 Ohshima T, Hijikata M, Shimotohno K, Tsurumi T. 2009. TORC2, a coactivator of

cAMP-response element-binding protein, promotes Epstein-Barr virus reactivation from latency through interaction with viral BZLF1 protein. J Biol Chem 284:8033-41.

17. Schaeffner M, Mrozek-Gorska P, Buschle A, Woellmer A, Tagawa T, Cernilogar FM, Schotta G, Krietenstein N, Lieleg C, Korber P, Hammerschmidt W. 2019. BZLF1 interacts with chromatin remodelers promoting escape from latent infections with EBV. Life Sci Alliance 2.
18. Ramasubramanyan S, Osborn K, Flower K, Sinclair AJ. 2012. Dynamic chromatin environment of key lytic cycle regulatory regions of the Epstein-Barr virus genome. J Virol 86:1809-19.
19. Ramasubramanyan S, Osborn K, Al-Mohammad R, Naranjo Perez-Fernandez IB, Zuo J, Balan N, Godfrey A, Patel H, Peters G, Rowe M, Jenner RG, Sinclair AJ. 2015. Epstein-Barr virus transcription factor Zta acts through distal regulatory elements to directly control cellular gene expression. Nucleic Acids Res 43:3563-77.
20. Zhang Q, Hong Y, Dorsky D, Holley-Guthrie E, Zalani S, Elshiekh NA, Kiehl A, Le T, Kenney S. 1996. Functional and physical interactions between the Epstein-Barr virus (EBV) proteins BZLF1 and BMRF1: Effects on EBV transcription and lytic replication. J Virol 70:5131-42.
21. Nakayama S, Murata T, Murayama K, Yasui Y, Sato Y, Kudoh A, Iwahori S, Isomura H, Kanda T, Tsurumi T. 2009. Epstein-Barr virus polymerase processivity factor enhances BALF2 promoter transcription as a coactivator for the BZLF1 immediate-early protein. J Biol Chem 284:21557-68.
22. Durand DB, Shaw JP, Bush MR, Replogle RE, Belagaje R, Crabtree GR. 1988. Characterization of Antigen Receptor Response Elements within the Interleukin-2 Enhancer. Molecular and Cellular Biology 8:1715-1724.
23. Rao A. 1994. Nf-Atp - a Transcription Factor Required for the Coordinate Induction of Several Cytokine Genes. Immunology Today 15:274-281.
24. Jain J, Mccaffrey PG, Valgeareher VE, Rao A. 1992. Nuclear Factor of Activated T-Cells Contains Fos and Jun. Nature 356:801-804.
25. Matsuda G, Nakajima K, Kawaguchi Y, Yamanashi Y, Hirai K. 2003. Epstein-Barr virus (EBV) nuclear antigen leader protein (EBNA-LP) forms complexes with a cellular anti-apoptosis protein Bcl-2 or its EBV counterpart BHRF1 through HS1-associated protein X-1. Microbiol Immunol 47:91-9.
26. Flower K, Hellen E, Newport MJ, Jones S, Sinclair AJ. 2010. Evaluation of a prediction protocol to identify potential targets of epigenetic reprogramming by the cancer associated Epstein Barr virus. PLoS One 5:e9443.
27. Lieberman PM, Berk AJ. 1991. The Zta trans-activator protein stabilizes TFIID association with promoter DNA by direct protein-protein interaction. Genes Dev 5:2441-54.
28. Pavlova S, Feederle R, Gartner K, Fuchs W, Granzow H, Delecluse HJ. 2013. An Epstein-Barr virus mutant produces immunogenic defective particles devoid of viral DNA. J Virol 87:2011-22.
29. Visalli RJ, Schwartz AM, Patel S, Visalli MA. 2019. Identification of the Epstein Barr Virus portal. Virology 529:152-159.
30. Henson BW, Perkins EM, Cothran JE, Desai P. 2009. Self-Assembly of Epstein-Barr Virus Capsids. Journal of Virology 83:3877-3890.

31. Goldfeld AE, Liu PF, Liu SF, Flemington EK, Strominger JL, Speck SH. 1995. Cyclosporine-a and Fk506 Block Induction of the Epstein-Barr- Virus Lytic Cycle By Antiimmunoglobulin. Virology 209:225-229.
32. Murata T. 2014. Regulation of Epstein-Barr virus reactivation from latency. Microbiol Immunol 58:307-17.
33. Bristol JA, Djavadian R, Albright ER, Coleman CB, Ohashi M, Hayes M, Romero-Masters JC, Barlow EA, Farrell PJ, Rochford R, Kalejta RF, Johannsen EC, Kenney SC. 2018. A cancer-associated Epstein-Barr virus BZLF1 promoter variant enhances lytic infection. PLoS Pathog 14:e1007179.
34. Zuo JM, Thomas WA, Haigh TA, Fitzsimmons L, Long HM, Hislop AD, Taylor GS, Rowe M. 2011. Epstein-Barr Virus Evades CD4(+) T Cell Responses in Lytic Cycle through BZLF1-mediated Downregulation of CD74 and the Cooperation of vBcl-2. Plos Pathogens 7.
35. Tierney RJ, Shannon-Lowe CD, Fitzsimmons L, Bell AI, Rowe M. 2015. Unexpected patterns of Epstein-Barr virus transcription revealed by a high throughput PCR array for absolute quantification of viral mRNA. Virology 474:117-30.
36. Ben-Bassat H, Goldblum N, Mitrani S, Klein G, Johansson B. 1976. Concanavalin A receptors on the surface membrane of lymphocytes from patients with African Burkitt's lymphoma and lymphoma cell lines. Int J Cancer 17:448-54.
37. Graham FL, Smiley J, Russell WC, Nairn R. 1977. Characteristics of a human cell line transformed by DNA from human adenovirus type 5. J Gen Virol 36:59-74.
38. Gallagher A, Armstrong AA, MacKenzie J, Shield L, Khan G, Lake A, Proctor S, Taylor P, Clements GB, Jarrett RF. 1999. Detection of Epstein-Barr virus (EBV) genomes in the serum of patients with EBV-associated Hodgkin's disease. International Journal of Cancer 84:442-448.
39. Godfrey A, Ramasubramanyan S, SInclair AJ. 2016. The use of chromatin precipitation coupled to DNA sequencing (ChIP-Seq) for the analysis of Zta binding to the human and EBV genome, Methods in Molecular Biology: Epstein-Barr virus, vol in press.
40. Dennis G, Jr., Sherman BT, Hosack DA, Yang J, Gao W, Lane HC, Lempicki RA. 2003. DAVID: Database for Annotation, Visualization, and Integrated Discovery. Genome Biol 4:P3.

Figure Legends

Figure 1. Identification of the Zta-interactome in Akata cells undergoing EBV lytic replication.

Akata cells were induced to initiate EBV replication by exposure to IgG for 24 hours.

A. Zta protein expression was validated by western blot analysis with the antibodies for the indicated proteins. The migration of molecular weight markers (kD) is shown on the left.

B. Induction of EBV lytic replication was assessed using Q-PCR to determine the change in EBV genome load in the cells. ** p≤0.01.

C. The immunoprecipitates for each of the triplicates in each arm of the study were analyzed by western blot for Zta protein.

D. A DSP-crosslinked protein extract was isolated following treatment with DNAse. Following immunoprecipitation with control of Zta-specific antibodies, proteins were subject to TMT-labelling and mass spectrometry. The abundance changes are shown on a scatter plot relative to each control (log_2). Those shown in green were enriched ≥2 fold for with respect to either control.

E.

Figure 2. Zta interactome gene ontology analysis.

Gene ontology analysis of the 37 human proteins found that interact with Zta by mass spectrometry. The components of the most enriched group are shown in the chart (with p-value ≤0.001).

Figure 3. Association of NFATc2 with Zta in cells.

Akata cells were induced to lytic cycle for 24 hours following exposure to anti-IgG and proteins were extracted and analysed as 'Input'. Extracts were subject to

541 immunoprecipitation with the indicated antibodies and isotype controls then analysed by
542 western blotting for the proteins shown.

543 A. Immunoprecipitation antibody Zta
544 B. Immunoprecipitation antibody EBF1
545 C. Immunoprecipitation antibody LEF1

546 The migration of molecular weight markers (kD) is shown on the left.

547

548 **Figure 4. No impact of calcium signaling pathway on transcriptional activation by Zta in B-**
549 **cells**.

550 DG-75 B-cells were transfected with a Zta-reporter plasmid (BHLF1-luciferase) with and
551 without co-transfection of expression vectors for his Zta.

552 A. The ZRE driven reporter BHLF1-luciferase is shown with the location of six ZREs
553 indicated (as filled boxes).
554 B. Calcium signaling was stimulated or not through the addition of ionomycin/PMA. 48
555 hours later, cells were harvested for luciferase assay and western blot analysis.
556 Luciferase reporter assays were undertaken and the activation by hisZta or the
557 control vector, was normalized to total protein concentration. Error bars represent
558 the mean of triplicate readings ± SD.
559 C. Western blot analysis of Zta in B.
560 D. BHLF1-luciferase was co-transfected with Zta or control vector, and NFATc1 and
561 NFATc2 siRNA smart pool or non-targeting control siRNA by Neon electroporation in

562 DG-75 cells. Luciferase reporter assays were undertaken and the activation of hisZta
563 and control vector, normalized to total protein are shown.
564 E. Western blot analysis of the indicated proteins in D.
565 F. Following quantitation, the expression of NFATc1 is shown in black and for NFATc2 in
566 grey.

567 Error bars represent the mean of triplicate readings ± SD.

568 **Figure 5. Zta impact on NFAT transcription activity**.

569 pGL3-IL2 NFAT luciferase reporter construct was co-transfected with hisZta, a control vector
570 or Si RNA pools into DG75 cells. Ca^{2+} signaling was activated by ionomycin/PMA immediately
571 after transfection with the addition of the inhibitor FK506 as indicated. After 48 hours, cells
572 were harvested for luciferase reporter and western blot analysis.

573 A. The luciferase reporter promoter is shown. The NFAT ARRE2 elements are indicated
574 as filled boxes.
575 B. Luciferase assay showing the fold change in activity after Ionomycin/PMA
576 stimulation and impact of NFAT c1 and NFATc2 Si RNA.
577 C. Western blot showing the impact on NFATc1 and NFATc2 expression level.
578 D. Luciferase assay showing the fold change in activity after Ionomycin/PMA
579 stimulation, FK506 inhibition and impact of Zta expression.
580 E. Western blot showing Zta expression.

581 Error bars represent the mean of triplicate reads ± standard deviation (*) indicates $p<0.05$;
582 (**) indicates $p<0.01$; (*) indicates $p\leq0.05$.

583

584 **Figure 6. Zta bZIP domain interaction with a ZRE and the NFAT/ARRE2 element.**

585 The ability of GFP-tagged Zta bZIP domain to interact with the ARRE2 element was
586 compared to a ZRE element by electrophoresis mobility shift assay (EMSA).

587 A. The DNA sequence of each probe is shown with the known ZRE (underscored), the NFAT
588 element (bold) and the AP1 site (boxed) shown.

589 B. GFP and GFP-bZIP Zta proteins were produced and 1 µg analysed by staining.
590 C. The interaction of each GFP and GFP-bZIP Zta protein with the indicated ZREs are shown.
591 The relative level of complex is shown below each GFP-bZIP Zta lane.

592

593 **Figure 7. Impact of ionomycin, PMA and Zta on the IL2 promoter.**

594 The IL2 promoter and one ARRE2 element is shown (dark grey box) with location of
595 transcription factors (NFATc2 grey cube; AP1 filled circle; Zta open circle).

596 B. Following stimulation with ionomycin and PMA, transcription is activated through
597 the interaction of NFATc2 and AP1 at the ARRE2 element. This is blocked by the
598 FK506.
599 C. Following expression of Zta, transcription is activated to a lesser extent through an
600 indirect means that is not inhibited by FK506.

601 Combining stimulation with ionomycin and PMA and expression of Zta, transcription is
602 activated to an intermediate extent. FK506 reduces the expression to the level seen when

603 Zta is activation alone. Interaction of Zta with NFATc2 may account for the reduction in
604 impact of ionomycin and PMA stimulation.
605
606 **Table 1. Viral proteins in the Zta-interactome in Akata cells undergoing EBV lytic**
607 **replication.**
608 EBV proteins identified as part of the Zta-interactome in Akata cells are shown, together
609 with the fold change in abundance relative to each control ($p \leq 0.05$), the total number of
610 identified peptide spectra matched (psm) for the protein and the brief description of the
611 gene function.
612

Gene name	Description	Unique peptide	# PSMs	Ratio: compared to non-lytic	Ratio: compared to control antibody
BBRF1	Portal protein	1	1	28.82	10.21
BVRF2	Capsid scaffolding protein	12	15	13.12	4.88
BGLF4	Serine/threonine-protein kinase	5	5	11.54	2.28
BALF2	Major DNA-binding protein	17	18	11.77	2.26
BcLF1	Major capsid protein	17	18	10.72	2.42
BALF5	DNA polymerase	5	5	8.81	2.40
BMLF1	mRNA export factor ICP27 homolog	6	6	6.57	2.35

613

614 **Table 2. Cell proteins in the Zta-interactome in Akata cells undergoing EBV lytic**

615 **replication.**

616 Cell proteins identified as part of the Zta-interactome in Akata cells are shown, together

617 with the fold change in abundance relative to each control p≤0.05), the total number of

618 identified peptide spectra matched (psm) for the protein and the brief description of the

619 gene function.

Gene name	Description	Unique peptide	# PSMs	Ratio: compared to non-lytic	Ratio: compared to control antibody
FAM96B	Mitotic spindle-associated MMXD complex subunit MIP18	2	2	13.35	13.55
TMED9	Transmembrane emp24 protein transport domain containing 9	1	2	8.8	6.88
TIPRL	TIP41-like protein	2	2	7.74	7.14
NCOA5	Nuclear receptor coactivator 5	20	34	6.65	3.92
MMS19	MMS19 nucleotide excision repair protein homolog	7	7	6.47	8.05
TMED10	Full-length cDNA 5-PRIME end of clone CS0DF013YM24 of Fetal brain of Homo sapiens (Human) variant (Fragment)	2	2	6.33	5.37
FGFR2	Adenosylhomocysteinase	2	2	5.52	5.39

CIAO1	Probable cytosolic iron-sulfur protein assembly protein CIAO1	2	2	4.51	8.39
NFATC2	Nuclear factor of activated T-cells, cytoplasmic 2	6	6	3.37	2.8
HSPA8	Heat shock cognate 71 kDa protein (Fragment)	15	70	3.23	2.13
ARID1A	AT-rich interactive domain-containing protein 1A	4	4	3.09	3.23
RUNX3	Runt-related transcription factor	1	1	2.96	2.55
ADAMTSL1	ADAMTS-like protein 1	1	1	2.89	3.71
HSPA9	Stress-70 protein, mitochondrial	9	24	2.83	2.13
TLE3	Transducin-like enhancer protein 3	4	4	2.65	2.48
NFATC1	Nuclear factor of activated T-cells, cytoplasmic 1	5	6	2.63	2.35
TMED2	Transmembrane emp24 domain-containing protein 2	2	2	2.62	2.43
TAF6	Transcription initiation factor TFIID subunit 6	1	1	2.53	2.37
SRSF9	Serine/arginine-rich splicing factor 9	6	8	2.53	2.13
HMG20A	High mobility group protein 20A	2	2	2.51	2.20

PABPC1	Polyadenylate-binding protein 1	18	28	2.49	3.74
MEF2B	Myocyte-specific enhancer factor 2B	7	7	2.3	3.25
RBMXL1	RNA binding motif protein, X-linked-like-1	4	26	2.29	2.4
GATAD2B	cDNA FLJ37346 fis, clone BRAMY2021310, highly similar to Transcriptional repressor p66 beta	9	11	2.17	2.02
PABPC4	Polyadenylate-binding protein	12	19	2.16	2.61
YLPM1	YLP motif-containing protein 1	21	64	2.16	3.22
CPSF3L	Integrator complex subunit 11	4	4	2.11	2.45
KHDRBS1	KH domain-containing, RNA-binding, signal transduction-associated protein 1	14	47	2.09	3.00
RBMX	RNA-binding motif protein, X chromosome	9	36	2.09	2.02
TCF20	Transcription factor 20	23	24	2.07	2.21
SMARCD2	SWI/SNF-related matrix-associated actin-dependent regulator of chromatin subfamily D member 2	5	5	2.05	2.60
PHF14	PHD finger protein 14	14	15	2.05	2.21

620

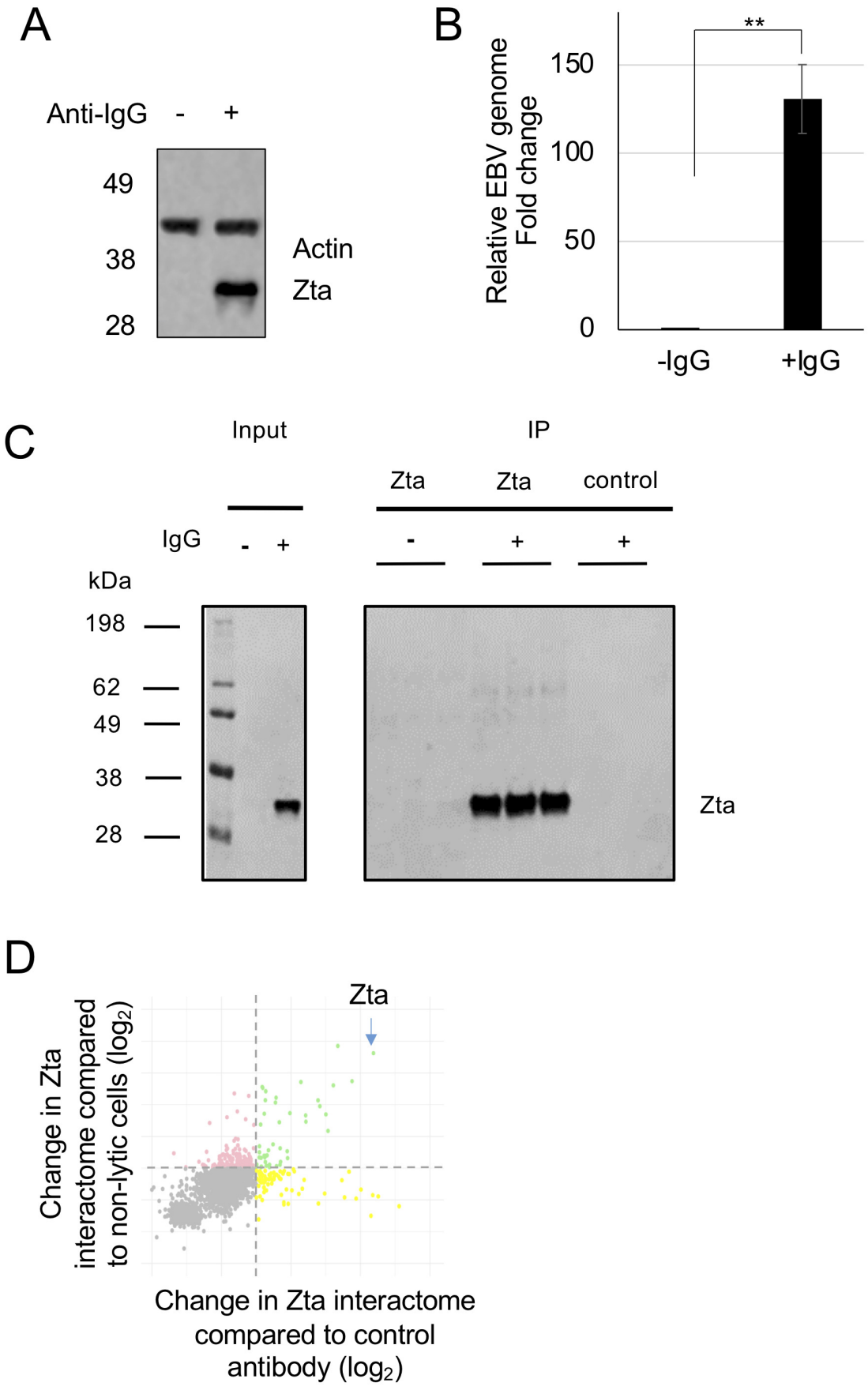

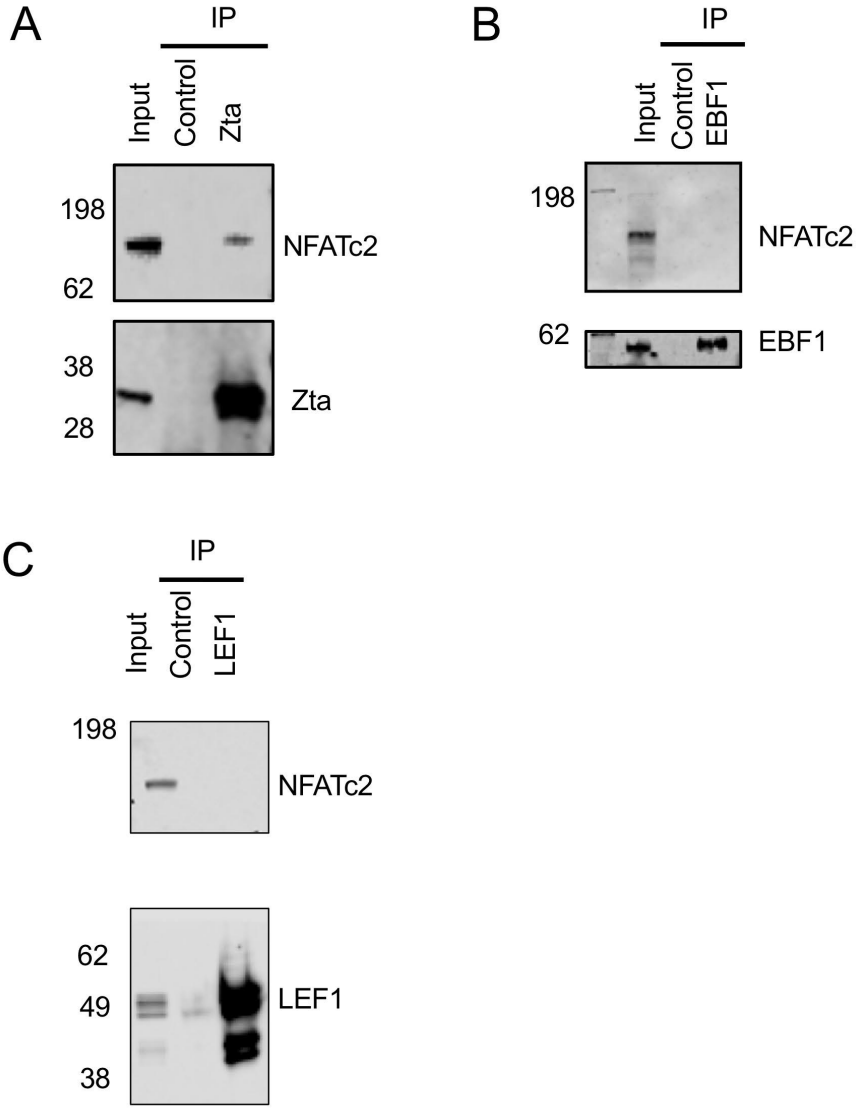

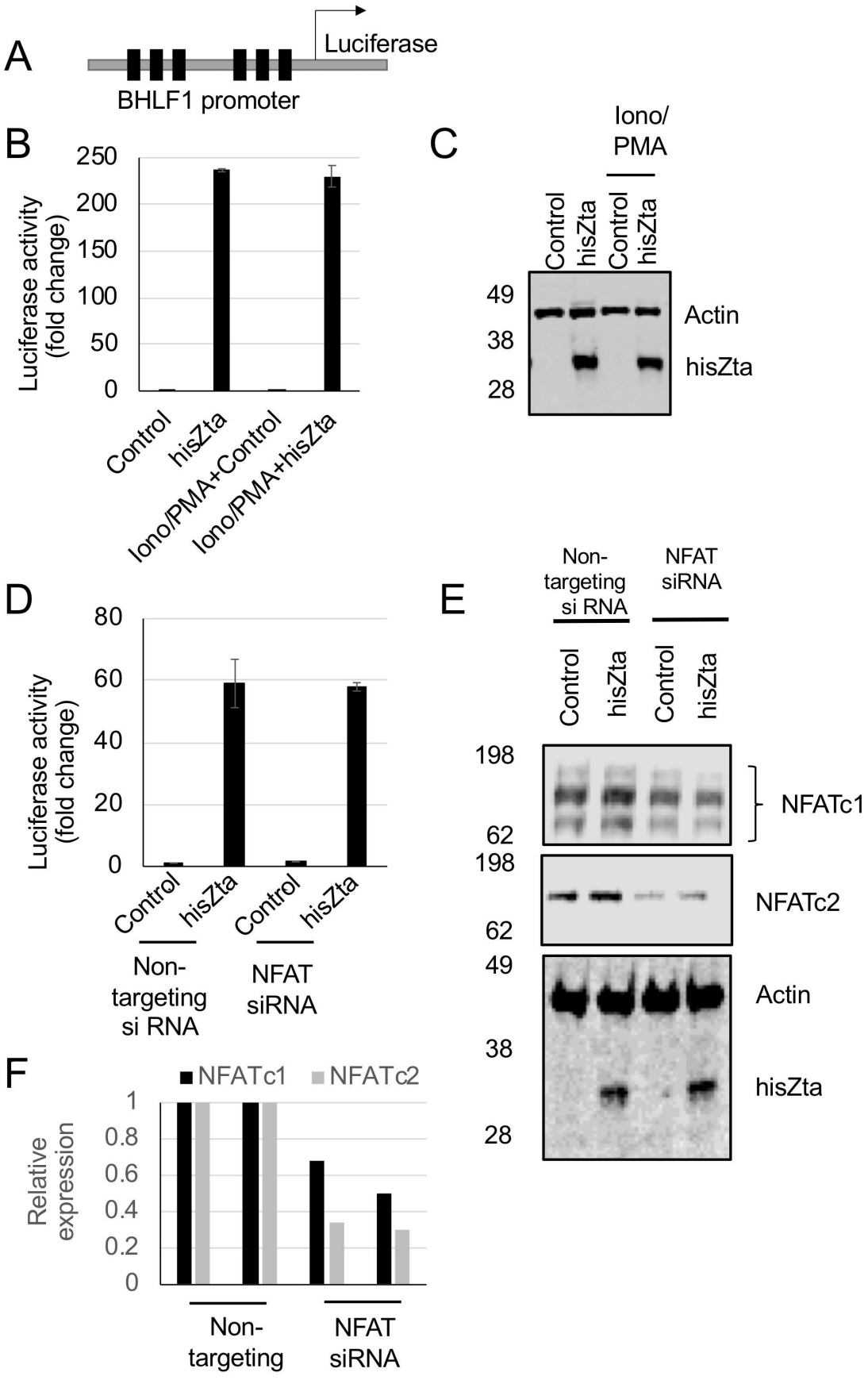

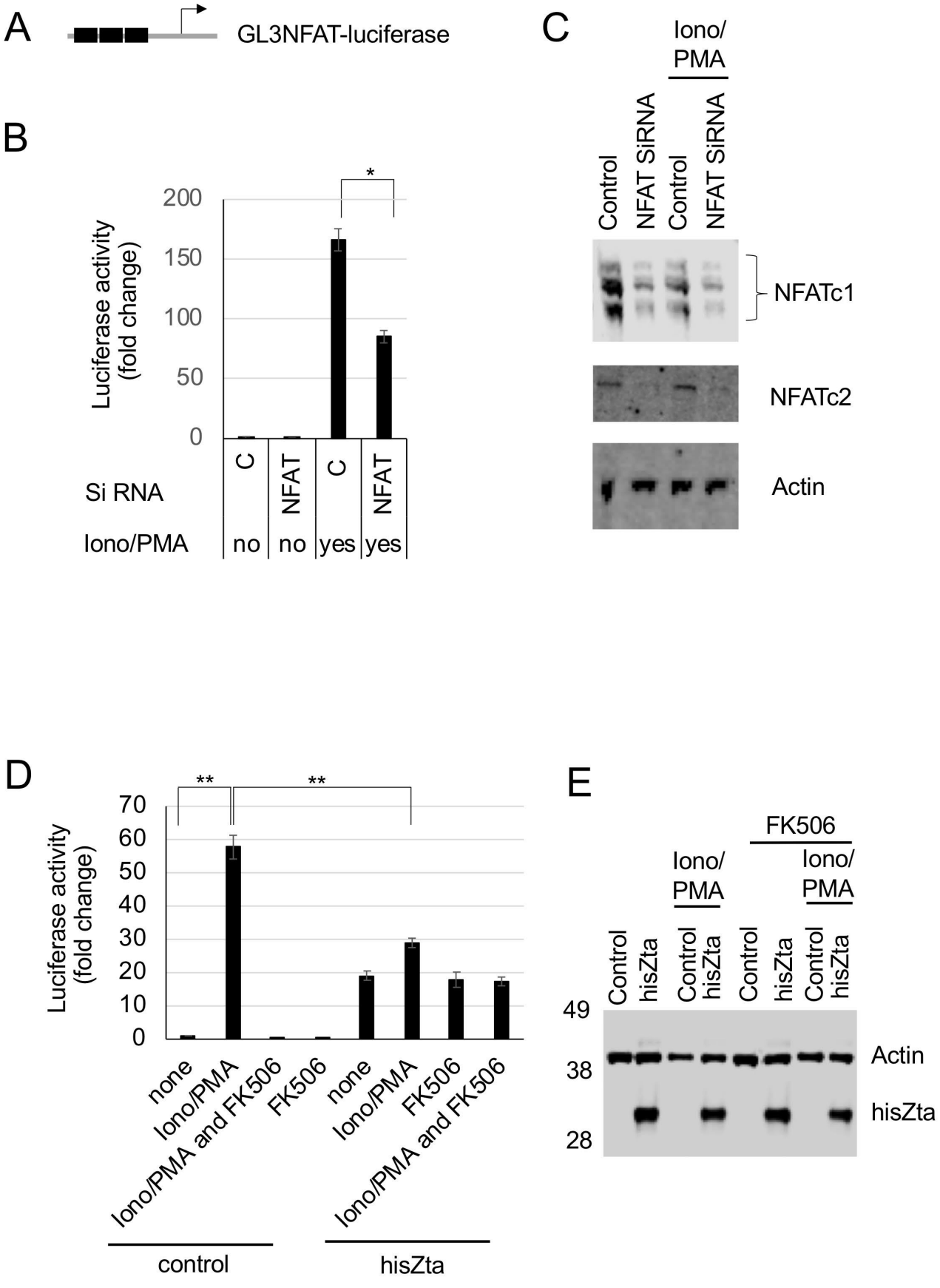

A

ZRE BMLF1 GAAGCACTGACTCATGAAG

NFAT/ARRE2 ACGCCTTCTGTATGAAACA**GTTTTTCC**TCC